Structural Consequences of Redesigning a Protein−Zinc Binding Site†

Joseph A. Ippolito and David W. Christianson*

Department of Chemistry, University of Pennsylvania, Philadelphia, Pennsylvania 19104−6323

Received June 28, 1994; Revised Manuscript Received September 24, 1994⊗

ABSTRACT: In order to probe the structural importance of zinc ligands in the active site of human carbonic anhydrase II (CAII), we have determined the three-dimensional structures of H94C (in metal-bound form), H94C-BME (i.e., disulfide-linked with β-mercaptoethanol), H94A, H96C, H119C, and H119D variants of CAII by X-ray crystallographic methods at resolutions of 2.2, 2.35, 2.25, 2.3, 2.2, and 2.25 Å, respectively. Each variant crystallizes isomorphously with the wild-type enzyme, in which zinc is tetrahedrally coordinated by H94, H96, H119, and hydroxide ion. The structure of H94C CAII reveals the successful substitution of the naturally occurring hisitidine zinc ligand by a cysteine thiolate, and metal coordination by C94 is facilitated by the plastic structural response of the β-sheet superstructure. Importantly, the resulting structure represents the catalytically active form of the enzyme reported previously [Alexander, R. S., Kiefer, L. L., Fierke, C. A., & Christianson, D. W. (1993) *Biochemistry 32*, 1510−1518]. Contrastingly, the structure of H96C CAII reveals that the engineered side chain does not coordinate to zinc; instead, zinc is tetrahedrally liganded by H94, H119, and two solvent molecules. Thus, the β-sheet superstructure is not sufficiently plastic in this location to allow C96 to coordinate to the metal ion. Substitution of the thiolate or carboxylate group for wild-type hisitidine in H119C and H119D CAIIs reveals that tetrahedral metal coordination is maintained in each variant; however, since there is no plastic structural response of the corresponding β-strand, a longer metal−ligand separation results. Finally, the crystal structures of H94C-BME and H94A CAIIs each reveal that zinc is dissociated from the active site. We conclude that H94 is vital for protein−metal affinity, and correlation of our structural data with functional measurements made by Kiefer and Fierke [Kiefer, L. L., & Fierke, C. A. (1994) *Biochemistry*, preceding paper in this issue] suggests that the plastic response of the metal coordination polyhedron or the protein scaffolding to metal ligand substitution contributes to attenuated protein−metal affinity.

Carbonic anhydrase II (CAII)[1] is a prototypical zinc metalloenzyme that catalyzes the interconversion of carbon dioxide and bicarbonate [for recent reviews, see Silverman and Lindskog (1988), Silverman (1991), Christianson (1991), and Lindskog and Liljas (1993)]. The three-dimensional structure of the human blood enzyme has been determined and refined at 1.54-Å resolution (Liljas et al., 1972; Håkansson et al., 1992) and shows zinc is liganded by the imidazole side chains of H94, H96, and H119; hydroxide ion completes a tetrahedral metal coordination polyhedron (Figure 1).

Genetic−structural studies of the avid zinc binding site of recombinant CAII [$K_d = 4 \times 10^{-12}$ M (Kiefer et al., 1993a)] allow us to dissect the contribution of molecular features responsible for protein−metal affinity and function; indeed, our initial studies reveal that the structure and chemistry of the protein-bound metal ion can be "fine-tuned" (Alexander et al., 1993; Kiefer et al., 1993a,b; Ippolito & Christianson, 1993). Since we and others use X-ray diffraction methods in our protein engineering experiments to directly visualize engineered metal sites [e.g., see Higaki et al. (1990), McGrath et al. (1993), Romero et al. (1993), and Browner et al. (1994)], the resulting structures provide a useful point of reference for the design of *de novo* metal sites in structurally uncharacterized proteins. Such systems include metalloantibodies (Iverson et al., 1990; Roberts et al., 1990; Wade et al., 1993), "minibodies" (Pessi et al., 1993), α-helical peptides (Ghadiri & Choi, 1990; Ruan et al., 1990), and α-helical bundles (Handel & DeGrado, 1990; Regan & Clarke, 1990).

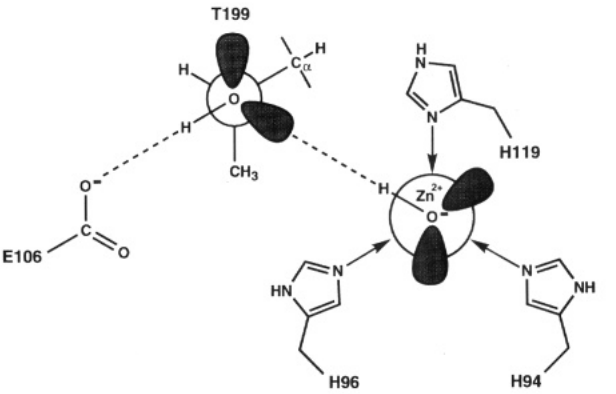

FIGURE 1: Zinc-binding site of wild-type CAII.

Here, we report the 2.2-Å resolution X-ray crystal structure of the metal-bound form of H94C CAII, in which the engineered cysteine thiolate coordinates to zinc by virtue of a moderately plastic β-sheet superstructure. In contrast, the structure of H96C CAII determined at 2.3-Å resolution reveals that the engineered cysteine thiolate does not interact with the zinc ion (which is liganded by H94, H119, and two

† This work is supported by a grant from the Office of Naval Research, and J.A.I. is supported in part by NIH Training Grant GM08275.

* Author to whom correspondence should be addressed.

⊗ Abstract published in *Advance ACS Abstracts,* November 15, 1994.

[1] Abbreviations: CAII, human carbonic anhydrase II; H94C, histidine-94→cysteine; H94C-BME, histidine-94→cysteine−β-mercaptoethanol complex; H94A, histidine-94→alanine; H96C, hisitidine-96→cysteine; H119C, histidine-119→cysteine; H119D, histidine-119→aspartate; BME, β-mercaptoethanol.

0006-2960/94/0433-15241$04.50/0

Table 1: Data Collection and Refinement Statistics for CAII Variants

	H94C CAII	H94C CAII-BME	H96C CAII	H119C CAII	H119D CAII	H94A CAII
number of crystals	1	2	1	1	1	1
number of measured reflections (2σ)	28 046	18 847	16 903	18 890	21 744	15 073
number of unique reflections	10 351	8563	9116	10 673	9283	8124
maximum resolution (Å)	2.2	2.35	2.3	2.2	2.25	2.25
R_{merge}[a]	0.059	0.075	0.088	0.088	0.076	0.081
number of water molecules in final cycle of refinement	105	135	111	113	129	103
number of reflections used in refinement (7.0 Å−max. resolution)	9130	7387	7746	10 014	8479	7807
completeness of data used in refinement (%)	76	73	75	83	76	68
R factor[b]	0.179	0.182	0.182	0.184	0.182	0.176
RMS deviation from ideal bond lengths (Å)	0.012	0.014	0.017	0.014	0.015	0.013
RMS deviation from ideal bond angles (deg)	1.8	2.3	2.3	1.8	1.6	2.5
RMS deviation from ideal planarity (Å)	0.005	0.005	0.007	0.006	0.006	0.005
RMS deviation from ideal chirality (Å^3)	0.085	0.082	0.089	0.087	0.089	0.089

[a] R_{merge} for replicate reflections, $R = \sum|I_{hi} - \langle I_h\rangle|/\sum\langle I_h\rangle$; I_{hi} = intensity measured for reflection h in data set i, $\langle I_h\rangle$ = average intensity calculated for reflection h from replicate data. [b] Crystallographic R factor, $R = \sum||F_o| - |F_c||/\sum|F_o|$; $|F_o|$ and $|F_c|$ are the observed and calculated structure factors, respectively.

solvent atoms), and no compensatory plastic response is oberved. Intermediate between these two extremes, the structures of H119C and H119D CAIIs reveal that tetrahedral metal coordination is maintained at the sole expense of longer metal−ligand separations and slight movements of the metal ion. Finally, we report the 2.35-Å resolution structure of the H94C CAII apoenzyme in which the C94 side chain is disulfide-linked with β-mercaptoethanol and the 2.25-Å resolution structure of the H94A CAII apoenzyme. These structures, along with those of other CAII variants already reported (Alexander et al., 1993; Ippolito & Christianson, 1993; Kiefer et al., 1993b), reveal the limited mutational plasticity of both the metal coordination polyhedron and the β-sheet superstructure into which the zinc binding site is nested.

EXPERIMENTAL PROCEDURES

Recombinant H94C, H94A, H96C, H119C, and H119D CAIIs were generously provided by Prof. Carol Fierke, Duke University. Crystals were prepared by minor modification of previously described procedures (Ippolito & Christianson, 1993). Crystals of metal-bound H94C CAII were prepared under anaerobic conditions in an argon glove bag (L. L. Kiefer, and C. A. Fierke, unpublished results). Thick, plate-like crystals of all CAII variants were grown at 4 °C with typical dimensions of 0.4 mm × 0.4 mm × 0.1 mm. All crystals were isomorphous with those obtained from the wild-type enzyme (space group $P2_1$ with unit cell parameters a = 42.7 Å, b = 41.7 Å, c = 73.0 Å, and β = 104.6°).

For data collection, crystals were immobilized and sealed in 0.5-mm glass capillaries, which were then mounted on Huber goniometers. With the exception of metal-bound H94C CAII, all diffraction data were measured on a Siemens X-100A multiwire area detector, mounted on a three-axis camera that was equipped with Charles Supper double X-ray focusing mirror. Cu Kα radiation was supplied by a Rigaku RU-200 rotating anode X-ray generator operating at 45 kV/50 mA. All data were collected at room temperature by the oscillation method. Raw data frames were processed using BUDDHA (Durbin et al., 1986), and replicate data were merged using PROTEIN (Steigemann, 1974) or CCP4 (distributed from the Daresbury Laboratory, Worrington WA4 4AD, U.K., 1991). For crystals of metal-bound H94C CAII, diffraction data were collected on an R-AXIS II image plate detector mounted on a Rigaku RU-300 rotating anode X-ray generator operating at 40 kV/80 mA. Raw intensities were integrated and reduced using the R-AXIS II PROCESS package. Pertinent data collection and reduction statistics for all experiments are recorded in Table 1.

The atomic coordinates of each CAII variant were refined against the X-ray data using the least squares algorithm PROLSQ (Hendrickson, 1985). The refined wild-type coordinates (Alexander et al., 1991), minus the side chain atoms corresponding to the mutated residue and all active site solvent atoms, comprised the starting model. In the case of H96C CAII, the zinc ion which is in the final structure was also omitted at the start of refinement. When the R factor dropped below 0.20, mutant side chains and solvent atoms were modeled into difference electron density maps generated by routines contained in X-PLOR (Brünger et al., 1987) with Fourier coefficients $|F_o| - |F_c|$ and phases calculated from the in-progress atomic model. Modeling was performed with the graphics software FRODO (Jones, 1985) installed on an Evans and Sutherland PS390 and with the graphics software CHAIN (Sack, 1989) and O (Jones et al., 1991) installed on a Silicon Graphics Indigo R4000. For each variant structure, refinement coverged smoothly to final crystallographic R factors within the range 0.176−0.184; all pertinent refinement statistics are recorded in Table 1. For each structure, the rms error in atomic positions was estimated to be ca. 0.2 Å based on relationships derived by Luzzati (1952). The atomic coordinates of each CAII variant have been submitted to the Brookhaven Protein Data Bank (Bernstein et al., 1977).

RESULTS

Despite local structural differences in their zinc binding sites, the overall structures of each CAII variant are quite similar: the rms deviation of C_α atoms between each CAII variant and the wild-type enzyme is 0.2 Å. In the remainder of this section, we outline the structural features of each engineered metal binding site which contribute to differences in protein−zinc affinity and catalytic activity.

H94C CAII. The difference electron density map of the metal-bound form of H94C CAII in Figure 2 reveals the desired $H_2C-Zn^{2+}(H_2O)$ site. This structure was stabilized

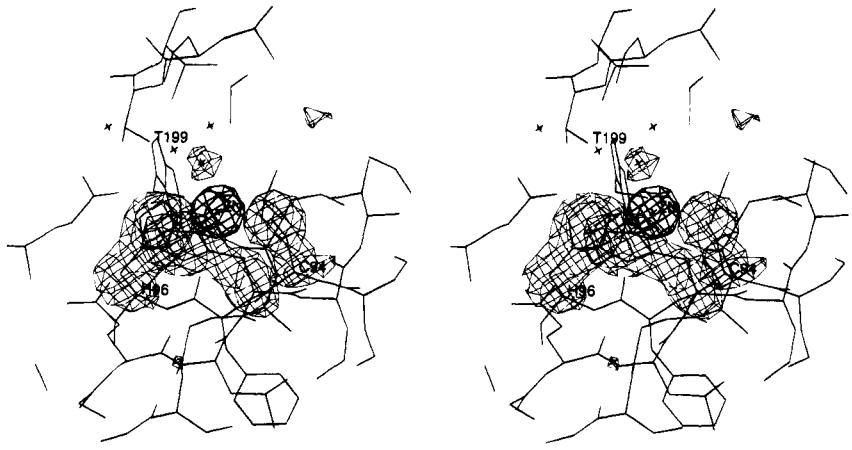

FIGURE 2: Difference electron density map of the metal-bound form of H94C CAII, generated with Fourier coefficients $|F_o| - |F_c|$ and phases calculated from the final molecule less the zinc-bound solvent molecule and the side chains of C94, H96, and H119. The map is contoured at 3σ, and the refined atomic coordinates of H94C CAII are superimposed. A map calculated with similar coefficients and phases from the final model less the active site zinc ion is contoured at 10σ in bold-faced density. C94, H96, T199, and zinc are indicated.

Table 2: Zinc−Ligand Distances in Wild-Type and Variant CAIIs (Å)

ligand	wild-type CAII[a]	H94C CAII	H96C CAII	H119C CAII	H119D CAII
residue 94	2.3	2.3	2.2	2.3	2.2
residue 96	2.1	2.3	6.1	2.1	2.0
residue 119	2.2	2.1	2.1	2.9	2.8
solvent #263	2.4	2.2	2.4	3.5	2.2
solvent #264			2.5		2.4

[a] Alexander et al. (1991).

only by the preparation of crystals under anaerobic conditions. The structure of the metal-bound variant is quite different from that of the metal-free variant reported earlier, which crystallizes in a different space group with an air-oxidized C94 side chain (Alexander et al., 1993). In the metal-bound structure, the engineered C94 thiolate coordinates to zinc with a Zn^{2+}−S separation of 2.3 Å. The geometry of the C94−zinc interaction is quite favorable, given that the $C_\alpha-C_\beta-S_\gamma-Zn^{2+}$ torsion angle of 99° is close to the preferred value of 90° tabulated from refined protein structures (Chakrabarti, 1989). Moreover, the χ_1 torsion angle for C94 is 55°, which is close to an energetically favorable value tabulated by Ponder and Richards (1987). We note that the C94 thiolate makes no hydrogen-bond interactions; this contrasts with the behavior of the engineered D94 zinc ligand in H94D CAII, to which the carboxyamide side chain of Q92 donates a hydrogen bond (Kiefer et al., 1993b). Zinc−ligand distances observed in H94C CAII are compared with those of the wild-type enzyme in Table 2. A comparison of metal-bound and metal-free H94C CAII structures is made in the Discussion section.

Given that the Zn^{2+}−S separation of 2.3 Å in H94C CAII is equal to the Zn−N separation of 2.3 Å in wild-type CAII, the structural implication is that the protein scaffolding compensates for the substitution of a smaller cysteine residue for a larger histidine metal ligand. This mutational plasticity involves the structure of both the metal coordination polyhedron as well as the core β-sheet superstructure. First, the zinc ion moves nearly 1 Å toward C94 with respect to its wild-type position. Second, the Y88−W97 β-strand flanking C94 is "pulled-out" from its wild-type position by about 1 Å to facilitate the coordination of C94 to zinc. This shift distorts, but does not break, interstrand hydrogen bonding within the β-sheet. The remaining protein ligands, H96 and H119, exhibit only minor conformational changes. It is remarkable that a slight deformation of the β-sheet accompanies C94−zinc coordination, and this structural change is highlighted in the least-squares superposition of H94C and wild-type CAIIs in Figure 3. Although this structural change presumably contributes to the significant attenuation of zinc affinity measured for H94C CAII relative to the wild-type enzyme [$K_d = 3.3 \times 10^{-8}$ M (Alexander et al., 1993)], the fact that protein−zinc affinity is similarly compromised in H94D (CAII [$K_d = 1.5 \times 10^{-8}$ M (Kiefer et al., 1993b)] suggests that the bulk of the energetic cost is incurred by the movement of the zinc rather than the deformation of the β-sheet. The active site zinc ion occupies the same position in H94C and H94D CAIIs; however, no β-sheet deformation is required for D94 to coordinate to zinc.

Finally, we note that the zinc-bound solvent is coordinated to the metal ion with a Zn^{2+}−O separation of 2.2 Å. We conclude that this is a water molecule and not hydroxide ion since its $pK_a \geq 9.5$ (Kiefer & Fierke, 1994). Zinc-bound water is also hydrogen bonded to the hydroxyl side chain of T199 with a somewhat short non-hydrogen atom separation of 2.4 Å. It is possible that this corresponds to a short, strong hydrogen bond (Cleland & Kreevoy, 1994), although this is not a principal structural feature of catalysis in the wild-type enzyme.

Prior to studying crystals of H94C CAII prepared under anaerobic conditions, we crystallized the protein in the presence of 3 mM β-mercaptoethanol (BME) in an attempt to hinder the air oxidation of C94. Difference electron density maps calculated with data collected from these crystals lack a strong peak in the active site corresponding to a bound zinc ion (data not shown). Moreover, additional electron density is found connected of C94, which we interpret as a disulfide linkage between the C94 side chain and a partially disordered BME molecule. The occurrence of BME−protein disulfide linkages is not unprecedented in cases where BME is present in the crystallization medium [e.g., see Eriksson et al. (1993)].

H96C CAII. The difference electron density map of the H96C CAII active site in Figure 4 reveals a fully occupied zinc ion bound to H94, H119, and two solvent molecules. Surprisingly, zinc moves 0.6 Å away from C96, and the engineered residue does not participate in zinc coordination

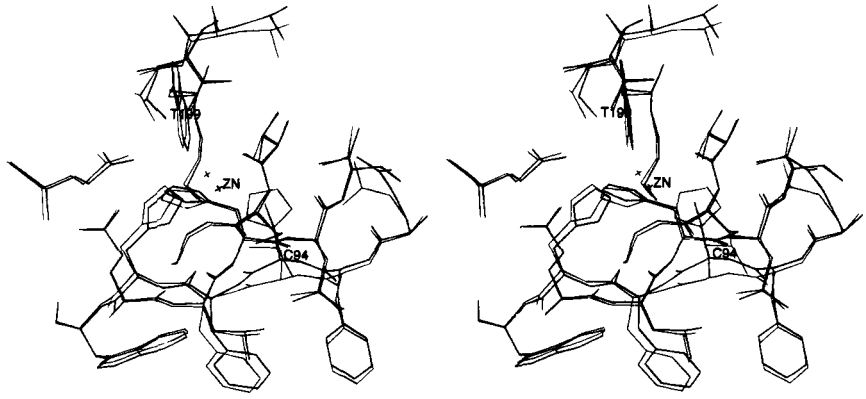

FIGURE 3: Least-squares superposition of H94C CAII (thick bonds) and wild-type (thin bonds) CAIIs. Residue 94, T199, and zinc are indicated. Solvent molecules have been omitted for clarity. Note that zinc moves toward C94; additionally, C94 and its associated polypeptide backbone moves toward zinc.

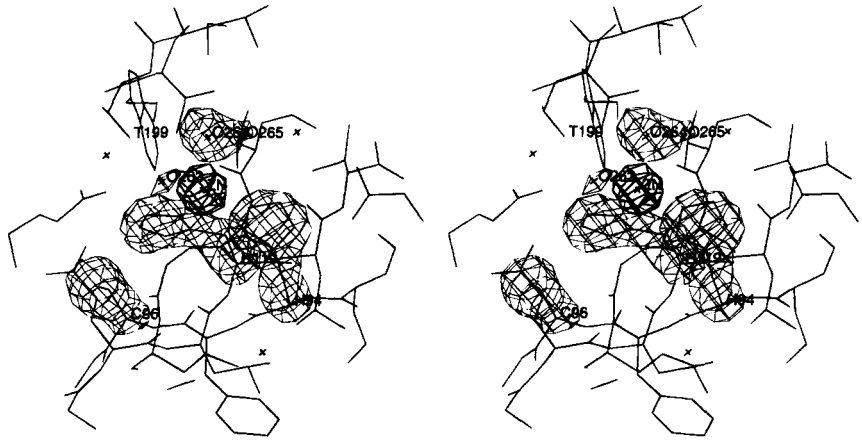

FIGURE 4: Difference electron density map (contoured at 3σ) of H96C CAII, generated with Fourier coefficients $|F_o| - |F_c|$ and phases calculated from the final model less the side chain atoms of H94, C96, and H119 and active site solvent molecules O263, O264, and O265. The bold-faced electron density corresponds to a difference Fourier calculation $|F_o| - |F_c|$ in which the phases are calculated from the final model less the active site zinc ion, and this map is contoured at 10σ. Both maps are superimposed upon the final refined coordinates; H94, C96, H119, T199, zinc, and solvent molecules are indicated. Alternatively, the electron density currently interpreted as waters 263, 264, and 265 may correspond to a disordered Tris molecule.

(Zn^{2+}−S separation = 6.1 Å). Additionally, C96 rotates by 113° about χ_1 away from the metal in order to occupy a small cavity resulting from the removal of the bulky H119 side chain. The unexpected conformation of C96 allows its thiol group to engage in a possible weak hydrogen bond with the backbone carbonyl oxygen of G104 (S−O separation = 3.4 Å). It is unlikely that the thiol side chain of C96 is ionized in this predominantly hydrophobic environment, particularly since the Zn^{2+}−S separation is so long.

Although zinc is only bound by two protein ligands, it still maintains tetrahedral coordination geometry due to the presence of two nonprotein ligands in its coordination polyhedron (Figure 4 and Table 2). However, we cannot ascertain the identity of these two nonprotein ligands with absolute certainty. Two water molecules (#264 and #265) are modeled into a broad electron density peak proximal to zinc in which water #264 coordinates to zinc with a Zn^{2+}−O separation of 2.5 Å. However, given that the refined separation of these two waters is only 2.0 Å, our current interpretation is not highly satisfactory. It is possible that this electron density peak corresponds to a disordered Tris molecule, the buffer present in the crystallization medium. Hence, the electron density peak corresponding to the second nonprotein zinc ligand (solvent #263, Zn^{2+}−O separation = 2.4 Å) could be another water molecule or another part of partially disordered, zinc-bound Tris. Although Tris does not bind to the zinc ion of wild-type CAII, we note that Tris−metalloprotein complexes have been reported in X-ray crystallographic studies of Hg^{2+}−carboxypeptides A (Rees et al., 1986) and Cu^{2+}−R96H trypsin (Higaki et al., 1990; McGrath et al., 1993).

The two nonprotein ligands participate in an array of hydrogen-bond interactions in the H96C CAII active site. Water molecule #263 is within hydrogen-bonding distance of the O_γ atom of T199 (2.5 Å) and the $O_\epsilon 1$ atom of E106 (2.8 Å). However, the $O_\epsilon 1$ atom of E106 also forms a 2.6-Å hydrogen bond with the O_γ atom of T199. Both interactions with the $O_\epsilon 1$ atom of E106 occur with *syn* stereochemistry. Finally, we note that zinc-bound water #264 does not engage in any hydrogen-bond interactions with protein residues.

The loss of a single protein ligand accounts for decreased protein−zinc affinity measured for H96C CAII relative to the wild-type enzyme ($K_d = 6.0 \times 10^{-8}$ M; Kiefer & Fierke, 1994). Although a zinc−thiolate interaction would be energetically favorable, the cysteine residue introduced at position 96 appears to be too constrained by its location in the β-sheet, i.e., the end of the Y88−W97 β-strand is sufficiently anchored such that it cannot distort to facilitate C96−metal coordination. Given that the engineered cysteine residue is much smaller than the histidine zinc ligand which it replaces, adequate plasticity in the protein scaffolding is required to achieve metal coordination in examples of

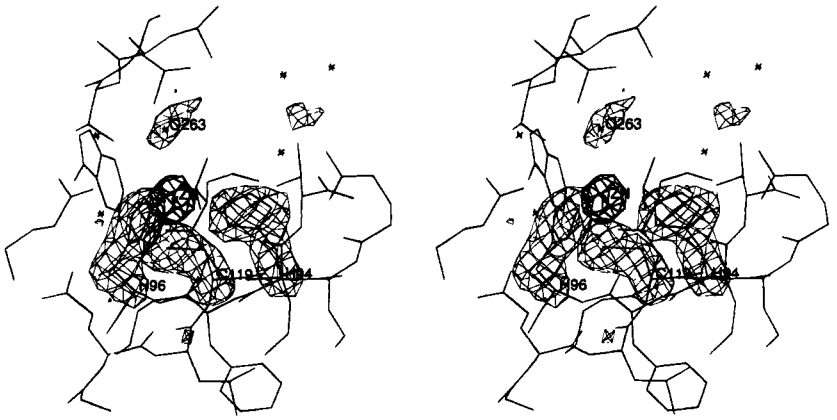

FIGURE 5: Difference electron density map of H119C CAII, generated with Fourier coefficients $|F_o| - |F_c|$ and phases calculated from the final model less the atoms of the zinc-bound solvent molecule and the side chains of H94, H96, and C119. The map is contoured at 3σ, and the refined atomic coordinates of H119C CAII are superimposed. The bold-faced electron density corresponds to a difference Fourier calculation (contoured at 10σ) in which the phases are calculated from the final model less the active site zinc ion. H94, H96, C119, zinc, and zinc-bound solvent are indicated. The C119−Zn^{2+} separation is 2.9 Å.

metalloprotein hisitidine→cysteine substitutions (e.g., as in the H94C CAII structure described previously): some regions of β-strands are more pliable than others in response to such substitutions.

H119C CAII. The difference electron density map of H119C CAII in Figure 5 reveals a zinc ion bound to H94, H96, C119, and one solvent molecule in a distorted tetrahedral array. Even though the zinc ion moves 0.2 Å toward the C119 side chain, the C119 thiolate−Zn^{2+} separation of 2.9 Å is much longer than average [2.1 ± 0.2 Å; see Chakrabarti (1989)], which must contribute to weaker protein−metal affinity [$K_d = 4.8 \times 10^{-8}$ M; Kiefer & Fierke (1994)]. The χ_1 angle of C119 is −62°, which is close to the −57° χ_1 value of H119 in wild-type CAII and is near the optimal value tabulated by Ponder and Richards (1987). The $C_\alpha-C_\beta-S_\gamma-Zn^{2+}$ torsion angle of 161° indicates that metal coordination occurs with roughly *trans* stereochemistry. Thus, with the exception of a longer-than-average sulfur−zinc separation, the stereochemistry and conformation of the substituted metal ligand are optimal. We note that the engineered C119 side chain makes no hydrogen-bond interactions with any other protein atoms, even though H119 donates a hydrogen bond to the side chain of E117 in the wild-type enzyme. The loss of this secondary interaction may also contribute to weaker zinc binding.

Solvent structure in the H119C CAII active site is somewhat disordered relative to that of the wild-type enzyme. In our current interpretation of the electron density map, we have modeled a single water molecule into the peak corresponding to the nonprotein zinc ligand. In the refined structure, this water exhibits a $Zn^{2+}-O$ separation of 3.5 Å, which is much too long for an inner-sphere interaction. It is possible that the crescent-shaped peak of electron density characterizing the nonprotein zinc ligand corresponds to a disordered Tris molecule. Moreover, we note that the refined thermal *B* factor of zinc is 24 Å^2, which is suggestive of partial occupancy. If the thermal *B* factor is held constant at 11 Å^2, the zinc occupancy refines to 0.71. These results suggest that zinc binding is destablized by the H119C substitution in the CAII active site, and this conclusion is consistent with the K_d of 4.8×10^{-8} M measured for this variant by Kiefer and Fierke (1994).

H119D CAII. The isosteric substitution of the N_δ atom of H119 with the O_δ atom of aspartate in the zinc coordination polyhedron might have been expected *a priori* to require minimal structural changes to maintain zinc coordination. However, the electron density map of H119D CAII reveals that the engineered side chain rotates away by 5° relative to the wild-type side chain such that the $Zn^{2+}-O$ separation is 2.8 Å (Figure 6). Carboxylate−zinc coordination occurs with unfavorable *anti* stereochemistry, and the $C_\gamma-O_\delta-Zn^{2+}$ angle is 138°; moreover, the zinc ion is 1.1 Å out of the plane of the carboxylate. Given the unfavorable zinc coordination stereochemistry and the zinc−carboxylate separation, we conclude that D119 destabilizes the zinc binding site relative to the wild-type enzyme.

H119D CAII exhibits well-ordered solvent structure around zinc. The electron density map of Figure 6 clearly indicates that two water molecules coordinate to zinc with $Zn^{2+}-O$ separations of 2.2 and 2.4 Å. Therefore, the zinc coordination polyhedron of H119D CAII is analogous to that of H96C CAII in that the metal is liganded by two inner-sphere protein atoms and two solvent atoms. In H119D CAII, both zinc-bound waters hydrogen bond with good stereochemistry to the hydroxyl side chain of T199 with nonhydrogen atom separations of 2.6 Å (water #263) and 2.9 Å (water #264). If the carboxylate oxygen of D119 is considered to be a weak axial fifth ligand, the zinc coordination polyhedron can be classified as a distorted trigonal bipyramid.

It is difficult to rationalize why the side chain of D119 moves away from the metal ion to form an unfavorable, *anti*-oriented zinc−carboxylate interaction. Furthermore, the side chain of E117 shifts slightly toward the metal site such that the E117 side chain is 2.8 Å away from the carboxylate group of D119. With this separation, it is likely that either the carboxylate side chain of E117 or D119 is protonated. Given that residue 119 is almost completely buried, perhaps a neutral histidine is better suited for this particular environment than a negatively charged aspartate residue. Although the histidine→aspartate substitution is isosteric with respect to the $N_\delta \rightarrow O_\delta$ zinc binding atom, it is not isosteric with respect to the size of the amino acid. Interestingly, when large buried residues are replaced by smaller ones in Cu,-Zn-superoxide dismutase, protein thermostability decreases, which is suggestive of unfavorable repacking interactions (McRee et al., 1990).

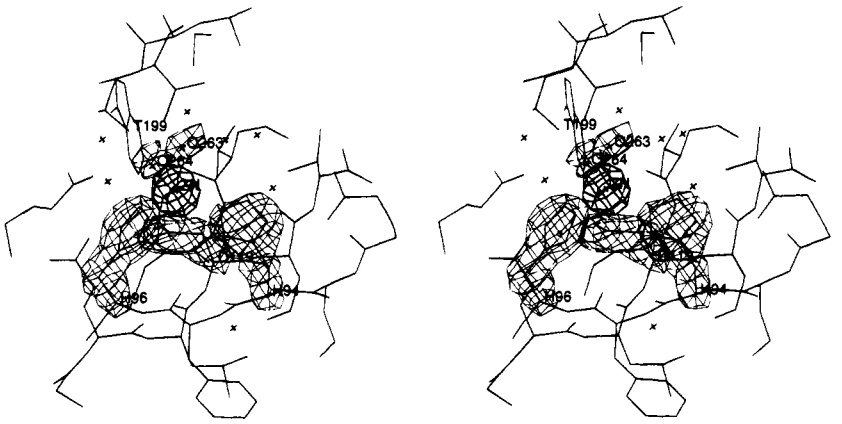

FIGURE 6: Difference electron density map of H119D CAII, generated with Fourier coefficients $|F_o| - |F_c|$ and phases calculated from the final model less the atoms of the two zinc-bound solvent molecules and the side chains of H94, H96, and D119. The map is contoured at 3.5σ, and the refined atomic coordinates of H119D CAII are superimposed. The bold-faced electron density corresponds to a difference Fourier calculation $|F_o| - |F_c|$ in which the phases are calculated from the final model less the active site zinc ion, and this map is contoured at 10σ. H94, H96, D119, T199, zinc, and the two zinc-bound solvents are indicated. The D119–Zn^{2+} separation is 2.8 Å.

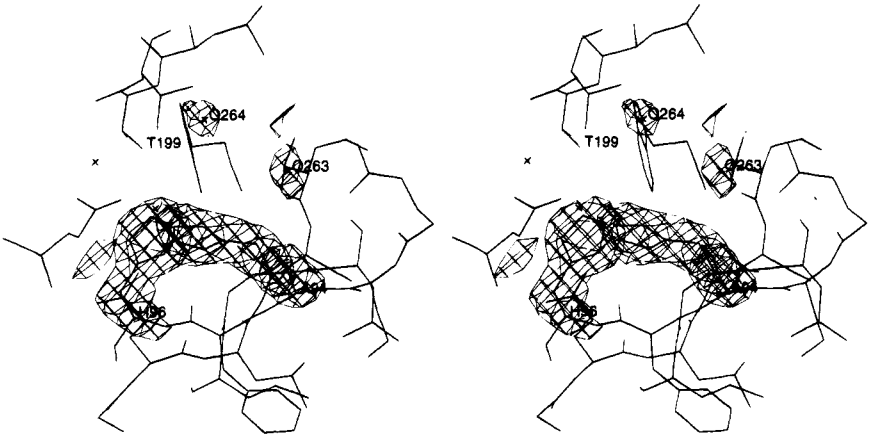

FIGURE 7: Difference electron density map of H94A CAII, generated with Fourier coefficients $|F_o| - |F_c|$ and phases calculated from the final model less the side chain atoms of A94, H96, H119, and active site water molecules #263 and #264. The map is contoured at 3σ; refined coordinates are superimposed, and A94, H96, T199, water #263, and water #264 are indicated. No electron density in the active site corresponds to a bound metal ion.

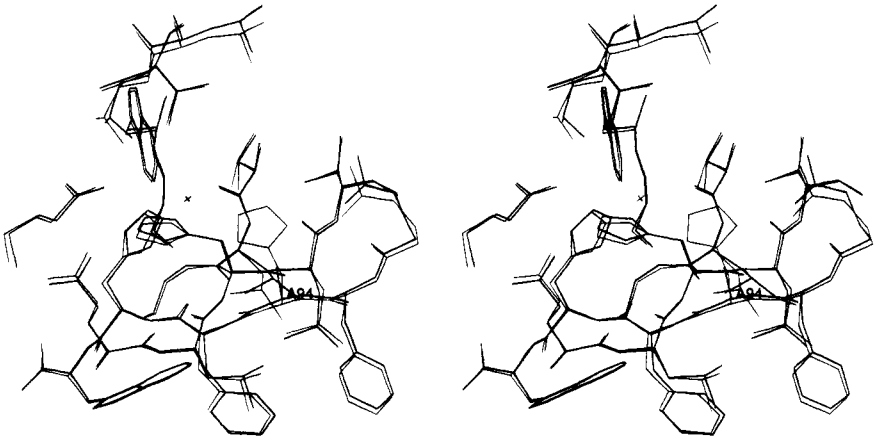

FIGURE 8: Least-squares superposition of H94A CAII (thick bonds) and wild-type (thin bonds) CAIIs; residue 94 is indicated. Note that the two structures are virtually identical, even though H94A CAII lacks a bound zinc ion.

H94A CAII. The difference electron density map of the H94A CAII active site reveals no peak corresponding to a bound zinc ion (Figure 7). Given that the variant binds zinc with $K_d = 2.7 \times 10^{-7}$ M (Kiefer & Fierke, 1994), it is likely that zinc dissociation is sufficiently facile under the high salt conditions of crystallization that a metal-free active site results. However, the structure of this metal-free variant is nonetheless informative: even though zinc is dissociated, all active site residues, including zinc ligands H96 and H119, superimpose extremely well upon their positions in the wild-type enzyme (Figure 8). Intriguingly, the void resulting from zinc dissociation contains no ordered solvent molecules. There is one new active site water molecule in H94A CAII that engages in a bidentate hydrogen bond with the side chain of Q92, which in wild-type CAII, hydrogen bonds to H94. We also note that a well-ordered solvent molecule (water

#264) hydrogen bonds to both the hydroxyl group and the backbone NH group of T199. This solvent molecule is located between the refined positions of zinc-bound hydroxide and the so-called "deep" water molecule in the active site of the wild-type enzyme.

The apparent rigidity of the histidine metal ligands in H94A CAII must be attributed to (1) strong hydrogen bonds involving the histidine ligands (Christianson & Alexander, 1989, 1990) and (2) the stability of the β-sheet superstructure in which the Y88−W97 strand is nested. Thus, air oxidation (Alexander et al., 1993) or metal-binding of C94 is sufficient to "pull out" its flanking polypeptide strand from the β-sheet, but the simple dissociation of zinc or BME-oxidation of C94 is not sufficient to evoke a plastic structural response. This conclusion is consistent with the structure of the wild-type apoenzyme, in which neither the zinc ligands nor the polypeptide backbone of the Y88−W97 β-strand are reported to undergo a conformational change upon zinc dissociation (Håkansson et al., 1992).

DISCUSSION

Structural and Functional Importance of H94. The results of amino acid substitutions at positions 94 and 96 provide significant insight on the role of H94 in metal binding and catalysis. For example, although H94A CAII and H96C CAII each provide two remaining histidine side chains for metal complexation (H94 and H119 in H96C CAII, and H96 and H119 in H94A CAII), it is intriguing that only H96C CAII contains a fully bound zinc ion. Given that crystals of each variant are equilibrated under identical buffer conditions, the discrepancy in zinc binding must arise in part from subtle geometric and/or electrostatic differences between the pair of coordinating histidine residues in each variant. Additionally, the hydrogen-bond contacts of both nonprotein ligands in H96C CAII may confer additional stabilization on the metal complex in this variant. We note that H94 is the most solvent-exposed of the naturally occurring zinc ligands, located at the bottom of the conical active site cleft—this may explain why C94 in H94C CAII is much more prone to air oxidation (Alexander et al., 1993) than C96 of H96C CAII. Thus, the metal ligand at position 94 may play an important role in regulating zinc equilibration with solvent. If so, then the compromise of this key metal-binding residue by mutation (H94A CAII), chemical modification (H94C-BME CAII), or air oxidation (H94C CAII; Alexander et al., 1993) will facilitate the destabilization of the protein-metal complex and the loss of the metal ion to bulk solvent. Alternatively, if an amino acid side chain substituted for H94 is capable of facile metal ion coordination [e.g., as found for the variant side chains of H94D CAII (Kiefer et al., 1993b) and H94C CAII], this residue continues to perform its critical role of regulating zinc equilibration with solvent. However, this function will be attenuated depending on the energetic cost of the compensatory structural changes that accommodate metal coordination.

A complete discussion of structure−activity relationships in this series of CAII variants is found in the preceding paper in this issue by Kiefer and Fierke. On the basis of these measurements, we conclude that the catalytic importance of H94 is two-fold: (1) to maintain proper geometry of zinc, and therefore zinc-bound hydroxide, for attack at substrate CO_2, and (2) to maintain the optimal pK_a and reactivity of zinc-bound solvent for catalytic activity. Not surprisingly, the substitution of the neutral histidine imidazole with the negatively charged cysteine sulfhydryl group raises the pK_a of the zinc-bound water, and a nearly identical effect is observed in H94D CAII (Kiefer et al., 1993b). Clearly, the additional negative charge in the zinc coordination polyhedra of H94C and H94D CAIIs diminishes the ability of the metal ion to polarize its bound solvent molecule and stabilize the zinc−hydroxide form.

Mutational Plasticity of the β-Sheet Superstructure. Interestingly, varying degrees of plasticity are exhibited by the metal-binding CAII variants, and this behavior is largely confined to the Y88−W97 β-strand containing metal ligands His-94 and His-96. The term "plasticity" refers to the subtle rearrangements which accommodate an amino acid substitution in a protein structure and structural changes that can propagate for 10−15 Å away from the point of mutation (Perry et al., 1990; Alexander et al., 1991). Our work with the zinc binding site of CAII reveals a surprising degree of structural plasticity involving the annealing of the Y88−W97 β-strand within the greater β-sheet superstructure. We also note structural changes in the zinc coordination polyhedron itself, as the metal ion and its ligands compensate for amino acid substitutions of wild-type ligands.

The mutational plasticity of the Y88−W97 β-strand was initially observed in the structure of metal-free H94C CAII (Alexander et al., 1993). Here, C94 and its associated polypeptide chain move toward the vacated metal site by nearly 2 Å away from its annealed, wild-type conformation. Initially, this conformational change was believed to result from loss of zinc from the active site. However, a similar conformational change of the Y88−W96 β-strand is not observed in the metal-free structures of H94A or H94C-BME CAIIs, so this structural change cannot be linked exclusively with metal dissociation. Moreover, the movement of the Y88−W97 β-strand is also observed in the metal-bound form of H94C CAII, where the backbone movement facilitates the coordination of the C94 thiolate to zinc.

In contrast, no significant changes in the Y88−W97 β-strand are observed in the active site of H94D CAII (Kiefer et al., 1993b). The substitution of zinc ligand H94 by aspartate is accommodated solely by a ~1-Å shift of the zinc ion from its wild-type position toward the substituted side chain and slight rotations (<10°) of the χ_1 torsion angles of H96 and H119. Hence, the D94 side chain is sufficiently long to allow zinc coordination without requiring the Y88−W97 β-strand to "pull out" from the greater β-sheet superstructure. Given that position 94 lies within an extended β-strand, the additional free energy needed to displace C94 may contribute to the slightly diminished zinc affinity of H94C CAII ($K_d = 3.3 \times 10^{-8}$ M) in comparison with H94D CAII ($K_d = 1.5 \times 10^{-8}$ M). The active site zinc ion moves to identical locations in these two variants (within experimental error); thus, we estimate that the 0.9-Å movement of zinc costs a factor of 3.8×10^3 (5.0 kcal/mol) to protein−metal affinity. It follows that an additional factor of 2 (0.4 kcal/mol) is required to deform the β-sheet in the manner observed in H94C CAII. Slight deviations away from optimal metal binding stereochemistry for H96 and H119 may also contribute to this factor. Furthermore, the maximal cost to achieve β-sheet deformation at position 94 may be even less if the hydrogen bond between D94 and Q92 in H94D CAII contributes to protein−metal affinity.

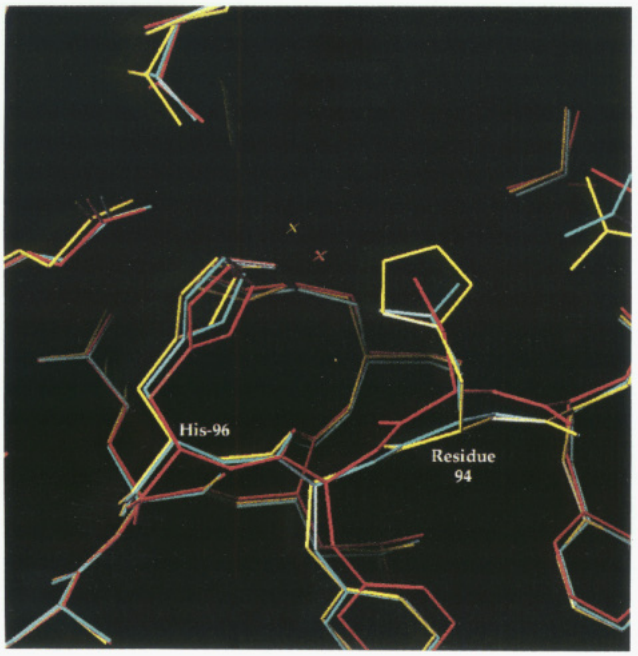

FIGURE 9: Least-squares superposition of the structures of wild-type CAII (yellow), H94D CAII (Kiefer et al., 1993b) (cyan), and H94C CAII (red). Residue 94 and H96 are indicated, and all solvent molecules have been omitted for clarity. Note that the zinc ion occupies the same nonnative site in both H94C and H94D CAIIs. Also note the movement of C94 and its flanking polypeptide backbone in H94C CAII with respect to the corresponding backbones of wild-type and H94D CAIIs.

The different structural changes in protein-zinc interactions accompanying amino acid substitutions at H94 are illustrated in Figure 9. When histidine is replaced with the smaller aspartate residue, the zinc cation shifts 1 Å toward the substituted side chain (Kiefer et al., 1993b). When the even smaller cysteine residue is substituted for histidine (recall that cysteine coordinates to metal through a S_γ atom), a 1-Å shift of zinc *and* a 1-Å shift of the entire cysteine residue are required for metal binding. Importantly, the zinc ion of H94D CAII superimposes upon that of H94C CAII within 0.1 Å, and this new zinc position reflects an energetically favorable state when the metal ion can still interact with all four ligands in a favorable, tetrahedral coordination polyhedron. The structures of H94A and H94C-BME CAIIs reveal that, without a favorable metal coordination interaction by residue 94, the deformation of the Y88−W97 β-strand has no molecular driving force. Parenthetically, we note that the structure of H94E has been determined by Xue and colleagues (1992), revealing a partially bound zinc ion and two conformations for the E94 side chain, and no conformational change of the Y88−W97 β-strand is observed.

The varying degrees of structural plasticity exhibited by H94C and H94D CAIIs are contrasted by the structural rigidity exhibited by H119C and H119D CAIIs. In H119C CAII, the zinc ion moves 0.2 Å toward C119, but the C119 backbone remains in its wild-type conformation. Resultantly, the cysteine−zinc separation of 2.9 Å is indicative of a weak interaction. The A116−N124 β-strand containing C119 is more buried than the Y88−W97 β-strand containing C94. Thus, it is reasonable that little structural plasticity is accessible to facilitate the coordination of C119 to zinc. Ultimately, the protein must balance the energetic cost of disrupting its internal structure with the formation of an optimal zinc−thiolate interaction; if the zinc ligand is sufficiently buried in the protein structure, then a plastic structural response facilitating zinc coordination would be too costly.

The structure of H119D CAII is surprising, in that the intuitive expectation is that D119 would superimpose perfectly with H119 and coordinate to zinc with *anti* stereochemistry without requiring any backbone adjustments; however, the X-ray structure reveals that the D119 side chain actually rotates away from the metal site. Apparently, D119 rotates toward the protein core in order to occupy the cavity resulting from the removal of the histidine imidazole ring. This suggests that the energetic cost of creating this particular cavity within the protein core is greater than the energy potentially gained by optimal carboxylate−zinc coordination.

SUMMARY AND CONCLUSIONS

This study demonstrates that the zinc binding site of CAII can be redesigned to accommodate other metal coordination motifs, which is the first step in conferring and modulating new catalytic functions. In particular, the structure of the metal-bound form of H94C CAII prepared under anaerobic conditions is the culmination of a series of genetic−structural analyses initiated to construct a $H_2C{-}Zn^{2+}$ site in the enzyme. Importantly, this work illuminates the plasticity of the β-sheet superstructure in accommodating amino acid substitutions in the zinc coordination polyhedron. The ultimate goal of this particular design thrust is to generate a metal coordination site of composition H_2CM, as found in blue copper proteins such as azurin (Norris et al., 1986; Nar et al., 1991), plastocyanin (Guss & Freeman, 1983), cupredoxin (Adman et al., 1989), and nitrate reductase (Godden et al., 1991).

We conclude the current study with the following key lessons:

(1) Despite a wide variety of ligand substitutions imposed upon the active site zinc ion in protein redesign experiments, the metal coordination polyhedron usually remains tetrahedral even if an additional nonprotein zinc ligand must be recruited from solvent.

(2) The redesigned metal binding site must ultimately display good stereochemistry. Whereas the engineered cysteine and aspartate ligands in H94C CAII and H94D CAII coordinate to zinc with optimal stereochemistry, the engineered ligands in the H119C and H119D CAII variants are constrained from doing so by their surroundings.

(3) When replacing a buried ligand, the effects of atomic volume and charge must be considered in addition to the intramolecular contacts of the ligand. The protein scaffolding may adjust to a radical ligand substitution in a manner that is unanticipated and possibly detrimental.

(4) β-Sheet structure and stability can be regulated through the construction of transition metal binding sites, and the architectural lessons presented herein may be applied to the engineering of metal sites on other β-saddle proteins such as serpins (Wei et al., 1994; C. A. Lesburg, and D. W. Christianson, unpublished results).

ACKNOWLEDGMENT

We thank L. Kiefer, C. Fierke, C. Lesburg, and S. Nair for helpful discussions. We also thank the Duke University

Medical Center, and in particular Dr. Stephen White, for use of their X-ray facility.

REFERENCES

Adman, E. T., Turley, S., Bramson, R., Petratos, K., Banner, D., Tsernoglou, D., Beppu, T., & Watanabe, H. (1989) *J. Biol. Chem. 264*, 87−99.

Alexander, R. S., Nair, S. K., & Christianson, D. W. (1991) *Biochemistry 30*, 11064−11072.

Alexander, R. S., Kiefer, L. L., Fierke, C. A., & Christianson, D. W. (1993) *Biochemistry 32*, 1510−1518.

Bernstein, F. C., Koetzle, T. F., Williams, G. J. B., Meyer, E. F., Brice, M. D., Rodgers, J. R., Kennard, O., Shimanouchi, T., & Tasumi, M. (1977) *J. Mol. Biol. 112*, 535−542.

Browner, M. F., Hackos, D., & Fletterick, R. (1994) *Nature Struct. Biol. 1*, 327−333.

Brünger, A. T., Kuriyan, J., & Karplus, M. (1987) *Science 235*, 458−460.

Chakrabarti, P. (1989) *Biochemistry 28*, 6081−6085.

Christianson, D. W. (1991) *Adv. Protein Chem. 42*, 281−355.

Christianson, D. W., & Alexander, R. S. (1989) *J. Am. Chem. Soc. 111*, 6412−6419.

Christianson, D. W., & Alexander, R. S. (1990) *Nature 346*, 225.

Cleland, W. W., & Kreevoy, M. M. (1994) *Science 264*, 1887−1890.

Durbin, R. M., Burns, R., Moulai, J., Metcalf, P., Freymann, D., Blum, M., Anderson, J. E., Harrison, S. C., & Wiley, D. C. (1986) *Science 232*, 1127−1132.

Eriksson, A. E., Cousens, L. S., & Matthews, B. W. (1993) *Protein Sci. 2*, 1274−1284.

Ghadiri, M. R., & Choi, C. (1990) *J. Am. Chem. Soc. 112*, 1630−1632.

Godden, J. W., Turley, S., Teller, D. C., Adman, E. T., Liu, M. Y., Payne, W. J., & LeGall, J. (1991) *Science 253*, 438−442.

Guss, J. M., & Freeman, H. C. (1983) *J. Mol. Biol. 169*, 521−563.

Håkansson, K., Carlsson, M., Svensson, L. A., & Liljas, A. (1992) *J. Mol. Biol. 227*, 1192−1204.

Handel, T., & DeGrado, W. F. (1990) *J. Am. Chem. Soc. 112*, 6710−6711.

Hendrickson, W. A. (1985) *Methods Enzymol. 115*, 252−270.

Higaki, J. N., Haymore, B. L., Chen, S., Flettrick, R. J., & Craik, C. S. (1990) *Biochemistry 29*, 8582−8586.

Ippolito, J. A., & Christianson, D. W. (1993) *Biochemistry 32*, 9901−9905.

Iverson, B. L., Iverson, S. A., Roberts, V. A., Getzoff, E. D., Tainer, J. A., Benkovic, S. J., & Lerner, R. A. (1990) *Science 249*, 659−662.

Jones, T. A. (1985) *Methods Enzymol. 115*, 157−171.

Jones, T. A., Zou, J.-Y., Cowan, S. W., & Kjeldgaard, M. (1991) *Acta Crystallogr. A47*, 110−119.

Kiefer, L. L., & Fierke, C. A. (1994) *Biochemistry 33*, 15233−15240.

Kiefer, L. L., Krebs, J. F., Paterno, S. A., & Fierke, C. A. (1993a) *Biochemistry 32*, 9896−9900.

Kiefer, L. L., Ippolito, J. A., Fierke, C. A., & Christianson, D. W. (1993b) *J. Am. Chem. Soc. 115*, 12581−12582.

Liljas, A., Kannan, K. K., Bergsten, P.-C., Waara, I., Fridborg, K., Strandberg, B., Carlbom, U., Järup, L., Lövgren, S., & Petef, M. (1972) *Nature New Biol. 235*, 131−137.

Lindskog, S., & Liljas, A. (1993) *Curr. Opin. Struct. Biol. 3*, 915−920.

Luzzati, P. V. (1952) *Acta Crystallogr. 5*, 802−810.

McGrath, M. E., Haymore, B. L., Summers, N. L., Craik, C. S., & Fletterick, R. J. (1993) *Biochemistry 32*, 1914−1919.

McRee, D. E., Redford, S. M., Getzoff, E. D., Lepock, J. R., Hallewell, R. A., & Tainer, J. A. (1990) *J. Biol. Chem. 265*, 14234−14241.

Nar, H., Messerschmidt, A., Huber, R., van de Kamp, M., & Canters, G. W. (1991) *J. Mol. Biol. 218*, 427−447.

Norris, G. E., Anderson, B. F., & Baker, E. N. (1986) *J. Am. Chem. Soc. 108*, 2784−2785.

Perry, K. M., Fauman, E. B., Finer-Moore, J. S., Montfort, W. R., Maley, G. F., Maley, F., & Stroud, R. M. (1990) *Proteins: Struct., Funct., Genet. 8*, 315−333.

Pessi, A., Bianchi, E., Crameri, A., Venturini, S., Tramontano, A., & Sollazzo, M. (1993) *Nature 362*, 367−369.

Ponder, J. W., & Richards, F. M. (1987) *J. Mol. Biol. 193*, 775−791.

Rees, D. C., Howard, J. B., Chakrabarti, P., Yeates, T., Hsu, B. T., Hardman, K. D., & Lipscomb, W. N. (1986) in *Zinc Enzymes* (Bertini, I., Luchinat, C., Maret, W., & Zeppezauer, M., Eds.) pp 155−166, Birkhäuser, Boston.

Regan, L., & Clarke, N. D. (1990) *Biochemistry 29*, 10878−10883.

Roberts, V. A., Iverson, B. L., Iverson, S. A., Benkovic, S. J., Lerner, R. A., Getzoff, E. D., & Tainer, J. A. (1990) *Proc. Natl. Acad. Sci. U.S.A. 87*, 6654−6658.

Romero, A., Hoitink, C. W. G., Nar, H., Huber, R., Messerschmidt, A., & Canters, G. W. (1993) *J. Mol. Biol. 229*, 1007−1021.

Ruan, F., Chen, Y., & Hopkins, P. B. (1990) *J. Am. Chem. Soc. 112*, 9403−9404.

Sack, J. S. (1988) *J. Mol. Graphics 6*, 224−225.

Silverman, D. N. (1991) *Can. J. Bot. 69*, 1070−1078.

Silverman, D. N., & Lindskog, S. (1988) *Acc. Chem. Res. 21*, 30−36.

Steigemann, W. (1974) Ph.D. thesis, Max-Planck-Institut für Biochemie, 8033 Martinsreid bei München, Germany.

Wade, W. S., Koh, J. S., Han, N., Hoekstra, D. M., & Lerner, R. A. (1993) *J. Am. Chem. Soc. 115*, 4449−4456.

Wei, A, Rubin, H., Cooperman, B. S., & Christianson, D. W. (1994) *Nature Struct. Biol. 1*, 251−258.

Xue, Y. (1992) *Structural and Functional Analyses of Active-Site Mutants of Human Isozyme II*, Doctoral Dissertation, University of Umeå, Umeå, Sweden.